Layered basic zinc acetate coating for dendrite-free Zn anode by interface environment regulation in aqueous zinc-ion batteries

Qingsong Cai[a], Zhenyu Guan[a], Yue Hu[a], Jianmin Zhang*[a], Kai Zhang*[b] and Zongmin Zheng*[a],

a. National Engineering Research Center for Intelligent Electrical Vehicle Power System, College of Mechanical and Electrical Engineering, Qingdao University, Qingdao, 266071, China.

b. Key Laboratory of Advanced Energy Materials Chemistry (Ministry of Education), College of Chemistry, Nankai University, Tianjin 300071, China

*Corresponding authors

Email: zhangjm@qdu.edu.cn; zhangkai_nk@nankai.edu.cn; zmzheng@qdu.edu.cn

Keywords: Zinc anode, Interface regulation, Coating, Aqueous zinc-ion battery

Fig. S1. Crystal structure (side view (a) and top view (b) in the layered structure) of the LBZA.

Fig. S2. (a) N_2 adsorption-desorption curve (b) Pore size distribution of LBZA powder.

Fig. S3. Statistical distribution of pore size of the LBZA powder.

Fig. S4. TEM image of the LBZA powder.

Fig. S5. Adhesion test of LBZA coating.

Fig. S6. SEM images of the LBZA@Zn electrode and the EDS elements mapping.

Fig. S7. Long-term cycling performance of LBZA@Zn symmetrical cells with different loadings at 0.5 mA cm^{-2} and 0.5 mAh cm^{-2}.

Fig. S8. Morphological changes to Bare Zn and LBZA@Zn soaked in an aqueous electrolyte solution (2 M $ZnSO_4$) for 7 days.

Fig. S9. Thickness comparison of Zn||Zn and LBZA@Zn||LBZA@Zn symmetric cells before and after cycling.

Fig. S10. Long-term cycling performance of the Zn||Zn and LBZA@Zn||LBZA@Zn symmetric cells under conditions of 0.5 mA cm^{-2} and 0.5 mAh cm^{-2}.

Fig. S11. Corresponding exchange current calculated based on the relationship between overpotential and current density.

Fig. S12. Discharge curves of Bare Zn and LBZA@Zn beaker-type batteries for 20 hours at 0.5 mA cm^{-2}.

Fig. S13. Digital pictures of Bare Zn electrode and LBZA@Zn electrode in beaker-type battery and after cycling.

Fig. S14. SEM images and corresponding EDS mapping images for the dendrite precipitate.

Fig. S15. SEM images and corresponding EDS mapping images for the by-product.

Fig. S16. XRD patterns of electrodes after one cycle of Zn||Zn and LBZA@Zn||LBZA@Zn beaker-type cells.

Fig. S17. The XPS spectra of Zn and LBZA@Zn anode for 100 cycles at 1 mA cm^{-2} and 1 mAh cm^{-2} : (a) C 1s; (b) S 2p; (c) Zn 2p; (d) O 1s.

Fig. S18. Raman spectra of the LBZA@Zn electrode before and after cycling in a beaker-type cell.

Fig. S19. Schematic structure of $ZnSO_4$ aqueous solutions.

Fig. S20. EIS spectra of the symmetric cells at diverse temperatures and calculated E_a values.

Fig. S21. (a) CV curves and (b) EIS dots of Zn|| NVO and LBZA@Zn||NVO full cells.

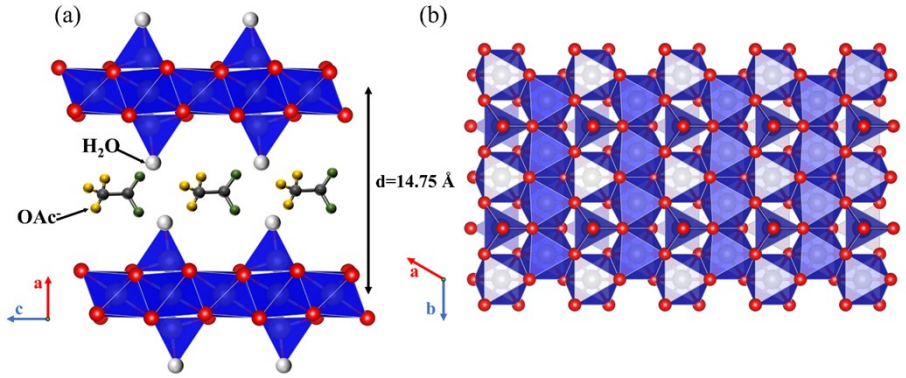

Fig. S1. Crystal structure (side view (a) and top view (b) in the layered structure) of the LBZA.

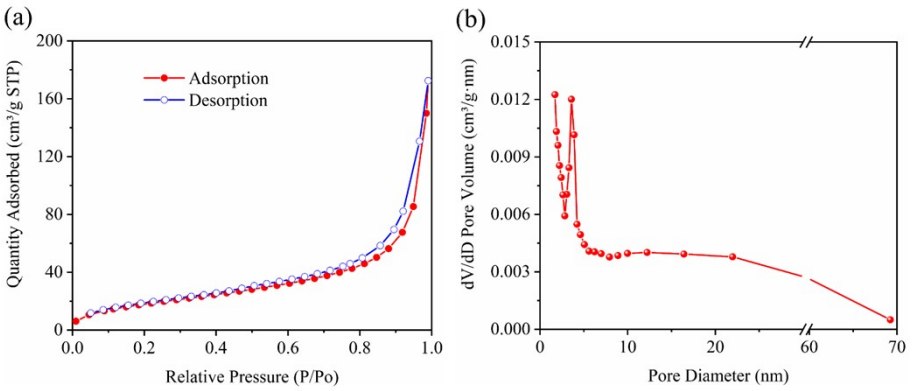

Fig. S2. (a) N_2 adsorption-desorption curve (b) Pore size distribution of LBZA powder.

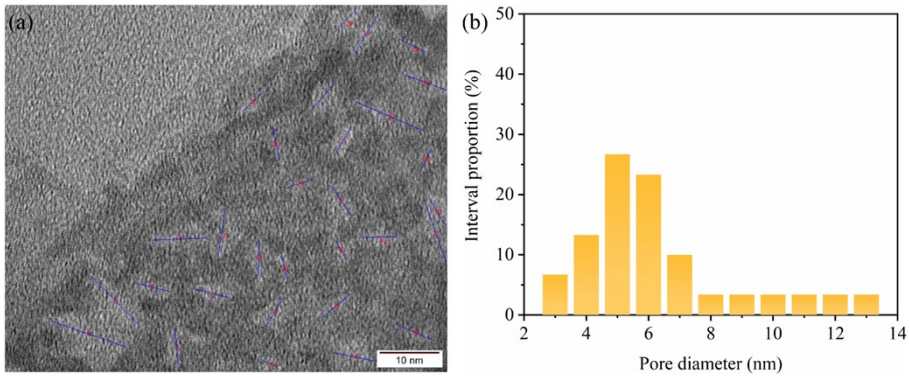

Fig. S3. Statistical distribution of pore size of the LBZA powder.

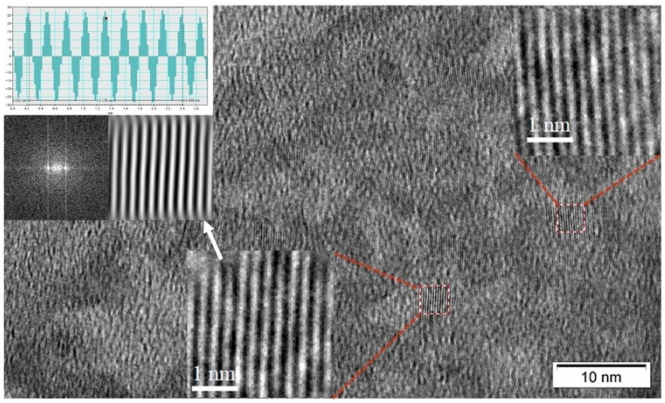

Fig. S4. TEM image of the LBZA powder.

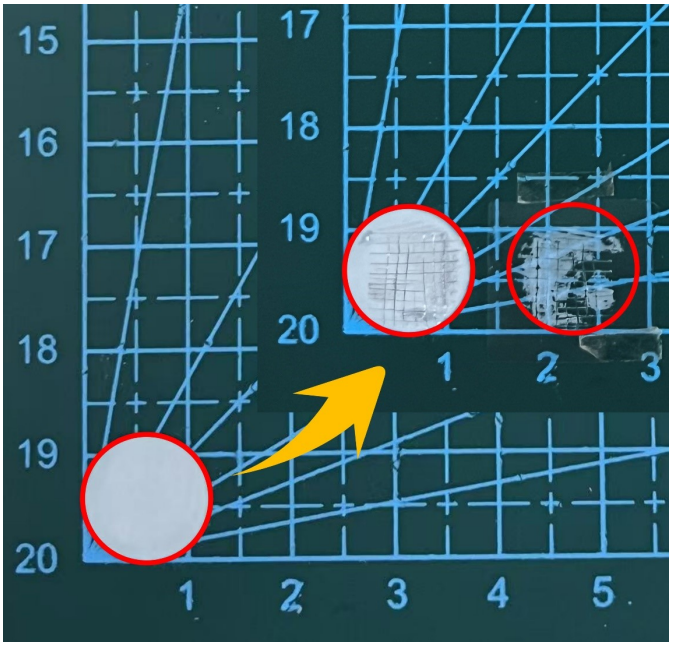

Fig. S5. Adhesion test of LBZA coating.

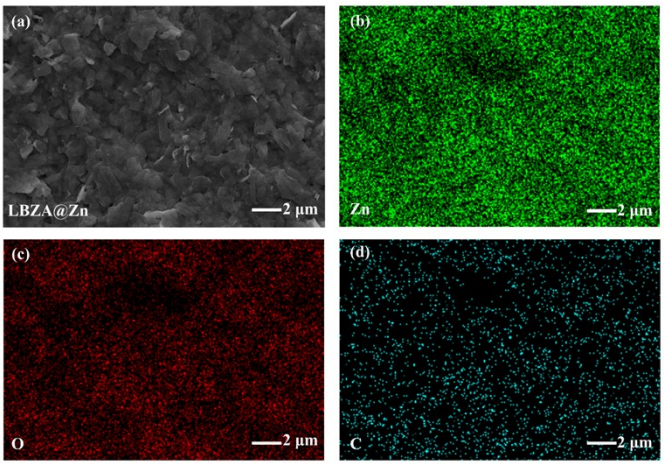

Fig. S6. SEM images of the LBZA@Zn electrode and the EDS elements mapping.

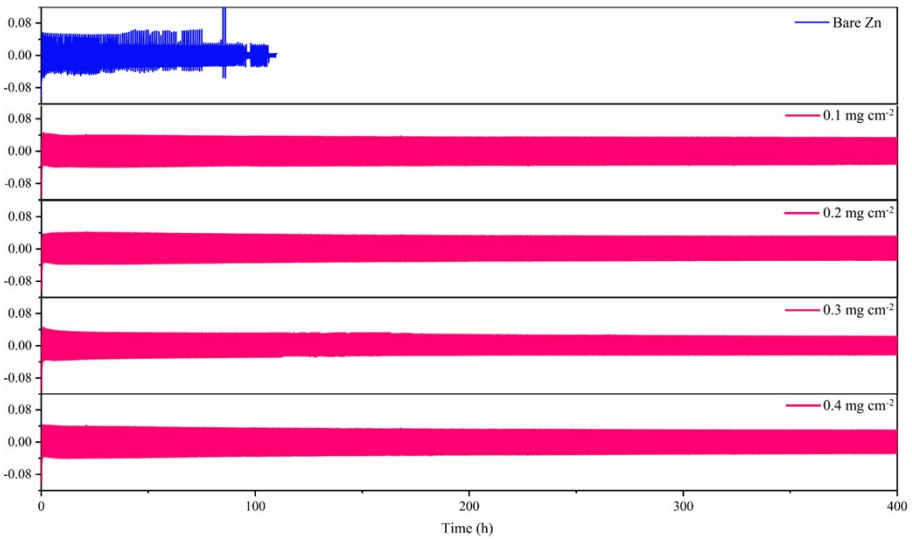

Fig. S7. Long-term cycling performance of LBZA@Zn symmetrical cells with different loadings at 0.5 mA cm^{-2} and 0.5 mAh cm^{-2}.

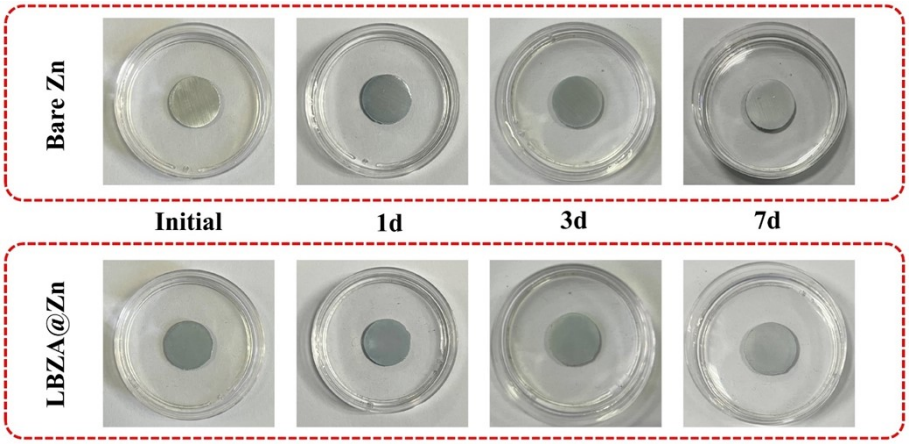

Fig. S8. Morphological changes to Bare Zn and LBZA@Zn soaked in an aqueous electrolyte solution (2 M $ZnSO_4$) for 7 days.

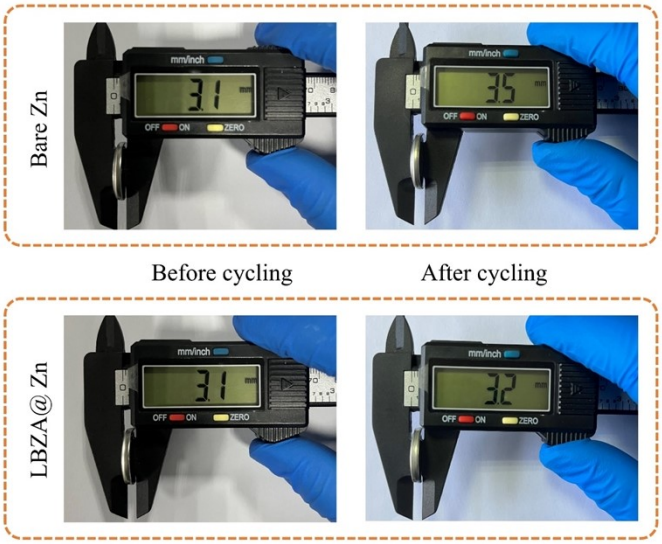

Fig. S9. Thickness comparison of Zn||Zn and LBZA@Zn||LBZA@Zn symmetric cells before and after cycling.

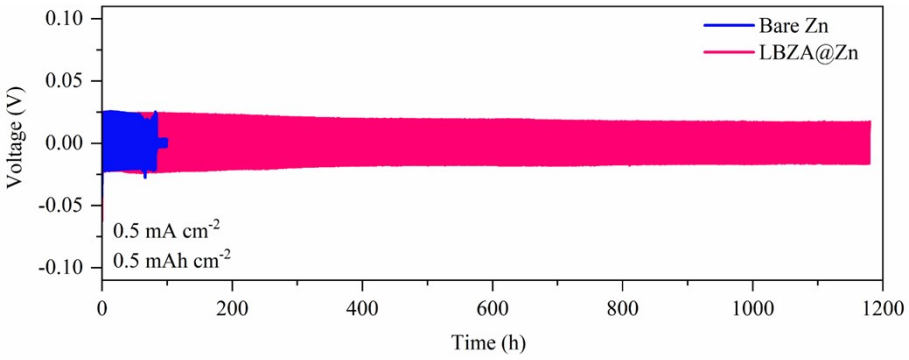

Fig. S10. Long-term cycling performance of the Zn||Zn and LBZA@Zn||LBZA@Zn symmetric cells under conditions of 0.5 mA cm^{-2} and 0.5 mAh cm^{-2}.

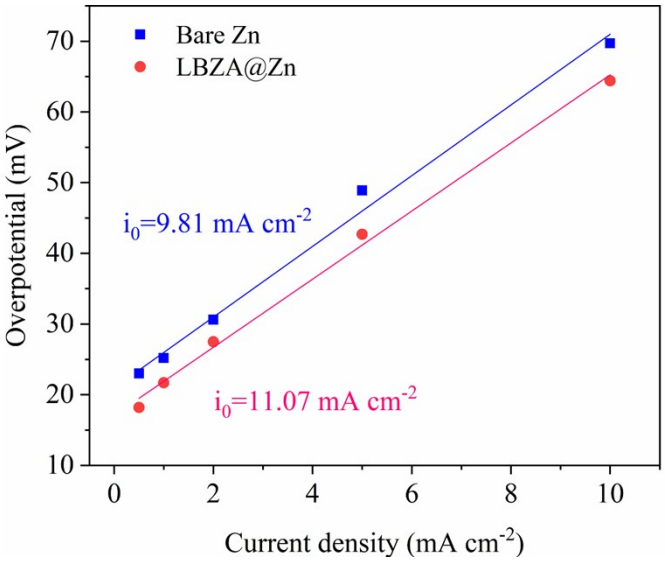

Fig. S11. Corresponding exchange current calculated based on the relationship between overpotential and current density.

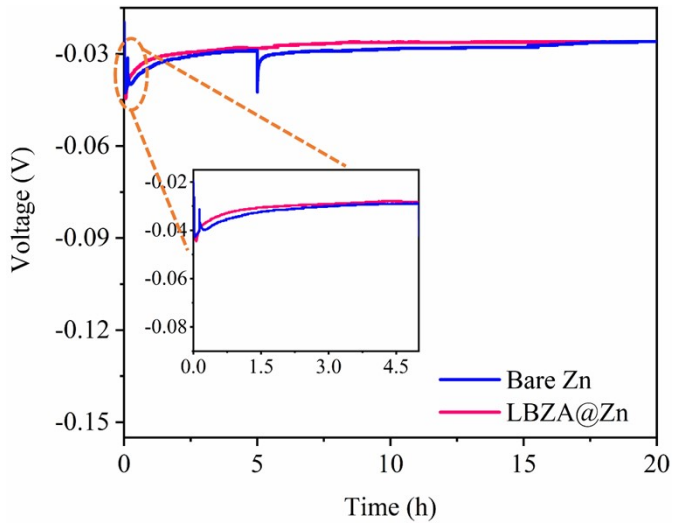

Fig. S12. Discharge curves of Bare Zn and LBZA@Zn beaker-type batteries for 20 hours at 0.5 mA cm^{-2}.

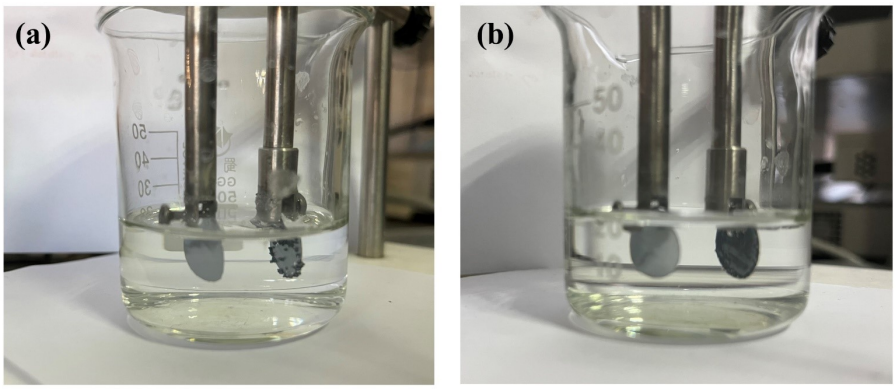

Fig. S13. Digital pictures of Bare Zn electrode and LBZA@Zn electrode in beaker-type battery and after cycling.

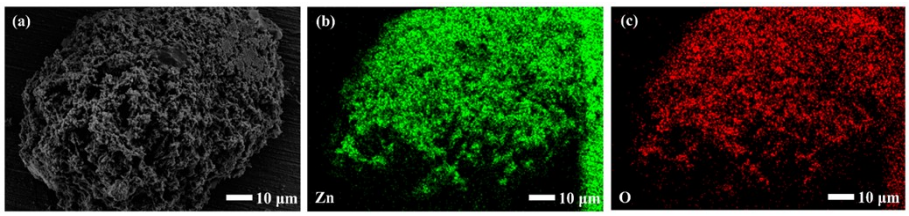

Fig. S14. SEM images and corresponding EDS mapping images for the dendrite precipitate.

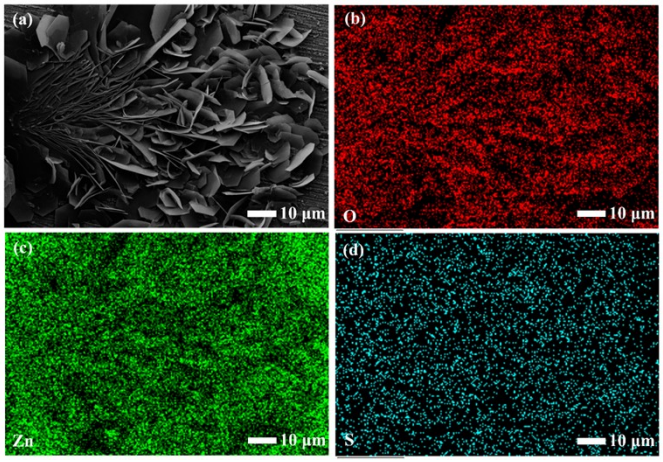

Fig. S15. SEM images and corresponding EDS mapping images for the by-product.

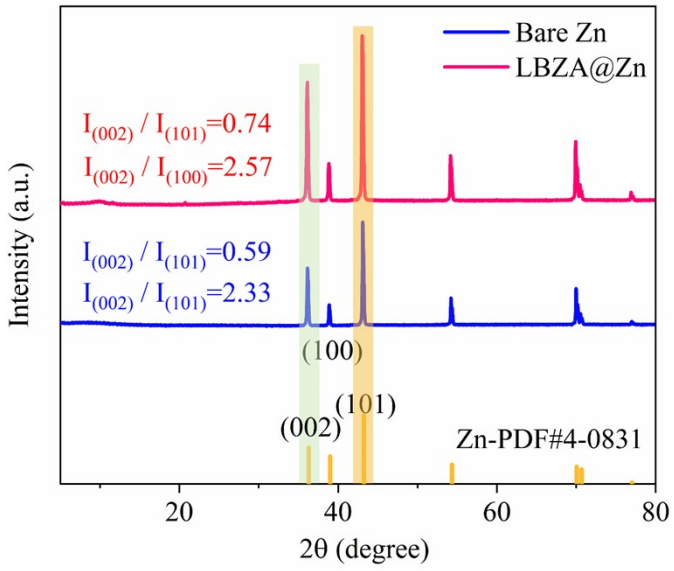

Fig. S16. XRD patterns of electrodes after one cycle of Zn||Zn and LBZA@Zn||LBZA@Zn beaker-type cells.

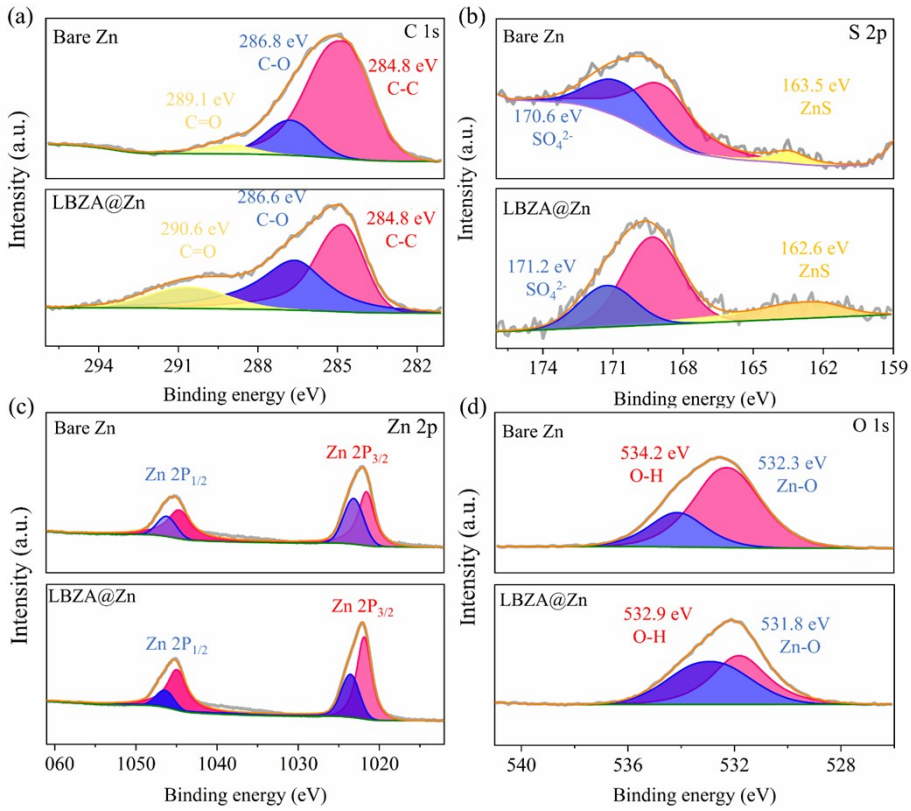

Fig. S17. The XPS spectra of Zn and LBZA@Zn anode for 100 cycles at 1 mA cm^{-2} and 1 mAh cm^{-2} :

(a) C 1s; (b) S 2p; (c) Zn 2p; (d) O 1s.

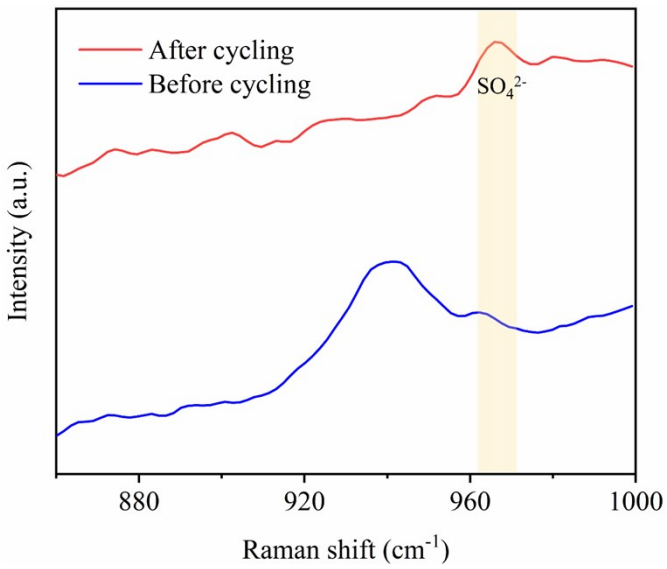

Fig. S18. Raman spectra of the LBZA@Zn electrode before and after cycling in a beaker-type cell.

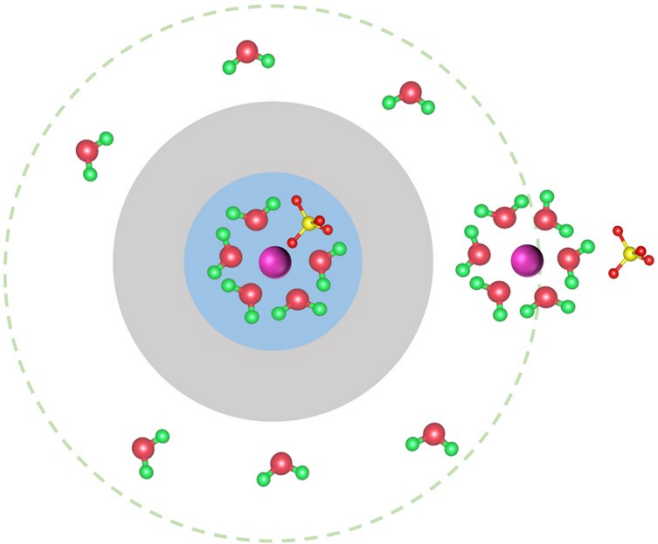

Fig. S19. Schematic structure of $ZnSO_4$ aqueous solutions.

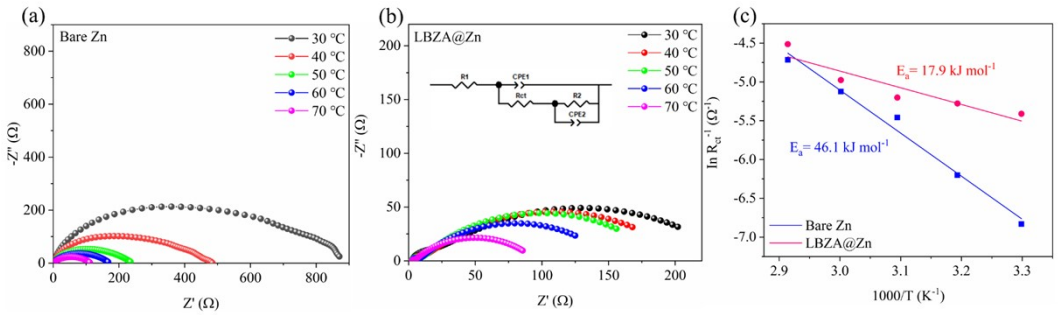

Fig. S20. EIS spectra of the symmetric cells at diverse temperatures and calculated E_a values.

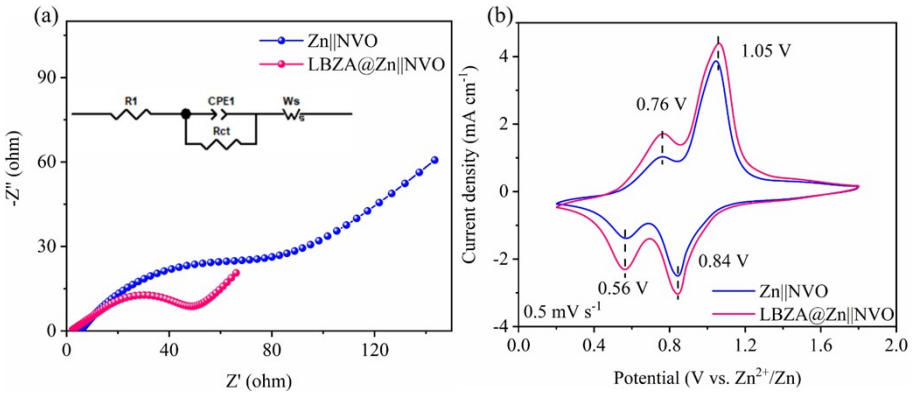

Fig. S21. (a) CV curves and (b) EIS dots of Zn|| NVO and LBZA@Zn||NVO full cells.

Table S1. Comparison of long-cycle performance of zinc anode symmetrical cells modified with different coatings.

Coating	Current density (mA cm^{-2})	Capacity (mAh cm^{-2})	Cycle time (h)	Ref.
LBZA@Zn	2	1	1800	This work
Ag-Zn	1	1	350	[1]
CaF2/Zn	3	1	600	[2]
Zn@CaF2	1	1	750	[3]
Zn@ZIF8	0.5	0.2	780	[4]
ISNF@CNTs@Zn	1	1	800	[5]
Zn@Bi	1.2	0.5	1000	[6]
PS-coated Zn	1	0.5	1000	[7]
PANZ@Zn	1	1	1145	[8]
GaIn@Zn	1	0.1	1200	[9]
ZnT-N-P@Zn	0.5	0.5	1200	[10]
PF@Zn	1	1	1400	[11]
Zn-SF	1	1	1400	[12]
c-PLA@Zn	1	1	1600	[13]
Tar-Zn	1	1	1600	[14]
ZnO-Zn	5	1	1762	[15]

Table S2. Comparison of asymmetric electric Coulombic efficiency (CE) performance of zinc anode modified by different coatings.

Coating	Current density (mA cm^{-2})	Capacity (mAh cm^{-2})	Cycle time (h)	Average CE (%)	Ref.
LBZA@Zn	1	0.5	5000	99.91	This work
Ta_2O_5@Zn	0.5	0.5	700	97.7	[16]
ANFZ@Zn	0.5	0.5	750	99.2	[17]
PDMS/TiO_{2-x}	0.5	0.5	900	99.4	[18]
Zn@CDs	0.5	0.5	2000	99.3	[19]
CNTguard-Ti	1	0.5	400	99.4	[20]
BTO/PVT@Zn	1	0.5	950	99.6	[22]
ZGL@Zn	1	0.5	1450	99.6	[21]
ZnT-N-P@Zn	1	1	280	99.6	[10]
Seo-OH@Cu	1	1	400	99.4	[23]
Zn-SF	1	1	500	99.2	[12]
ZnPO@Zn	1	1	800	99.8	[24]
InSnRZn	1	1	1600	99.5	[25]
HDSEI@Zn	1	1	1800	99.8	[26]
SA-Cu@Zn	1	1	1800	99.8	[27]
Porous PMMA-Cu	1	1	2000	99.8	[28]

REFERENCES

1 Q. Q. Lu, C. C. Liu, Y. H. Du, X. Y. Wang, L. Ding, A. Omar and D. Mikhailova, Uniform Zn Deposition Achieved by Ag Coating for Improved Aqueous Zinc-Ion Batteries, *ACS Appl. Mater. Interfaces*, 2021, **13**, 16869-16875.

2 Y. Feng, Y. D. Wang, L. Sun, K. Q. Zhang, J. C. Liang, M. F. Zhu, Z. X. Tie and Z. Jin, Fluorinated Interface Engineering toward Controllable Zinc Deposition and Rapid Cation Migration of Aqueous Zn-Ion Batteries, *Small*, 2023, **19**, 2302650.

3 Y. T. Li, S. N. Yang, H. X. Du, Y. Q. Liu, X. T. Wu, C. S. Yin, D. H. Wang, X. M. Wu, Z. X. He and X. W. Wu, A stable fluoride-based interphase for a long cycle Zn metal anode in an aqueous zinc ion battery, *J. Mater. Chem. A*, 2022, **10**, 14399-14410.

4 M. W. Cui, B. X. Yan, F. N. Mo, X. Q. Wang, Y. Huang, J. Fan, C. Y. Zhi and H. F. Li, In-situ grown porous protective layers with high binding strength for stable Zn anodes, *Chem. Eng. J.*, 2022, **434**, 134688.

5 J. M. Dong, J. W. Duan, R. R. Cao, W. Zhang, K. K. Fang, H. Yang, Y. Liu, Z. T. Shen, F. M. Li, R. Liu, M. Q. Jin, L. H. Lei, H. L. Li and C. Chen, Dendrite-free Zn deposition initiated by nanoscale inorganic–organic coating-modified 3D host for stable Zn-ion battery, *SusMat*, 2024, **4**, 189.

6 Y. X. Du, Y. Feng, R. T. Li, Z. Peng, X. Y. Yao, S. Y. Duan, S. D. Liu, S. C. Jun, J. Zhu, L. Dai, Q. Yang, L. Wang and Z. X. He, Zinc-Bismuth Binary Alloy Enabling High-Performance Aqueous Zinc Ion Batteries, *Small*, 2024, **20**, 2307848.

7 P. C. Zou, D. Nykypanchuk, G. Doerk and H. L. Xin, Hydrophobic Molecule Monolayer Brush-Tethered Zinc Anodes for Aqueous Zinc Batteries, *ACS Appl. Mater. Interfaces*, 2021, **13**, 60092-60098.

8 P. Chen, X. H. Yuan, Y. B. Xia, Y. Zhang, L. J. Fu, L. Liu, N. F. Yu, Q. H. Huang, B. Wang, X. W. Hu, Y. P. Wu, T. V. Ree and T. V. An, Artificial Polyacrylonitrile Coating Layer Confining Zinc Dendrite Growth for Highly Reversible Aqueous Zinc-Based Batteries, *Adv. Sci.*, 2021, **8**, 2100309.

9 C. Liu, Z. Luo, W. T. Deng, W. F. Wei, L. B. Chen, A. Q. Pan, J. M. Ma, C. W. Wang, L. M. Zhu, L. L. Xie, X. Y. Cao, J. G. Hu, G. Q. Zou, H. S. Hou and X. B. Ji, Liquid Alloy Interlayer for Aqueous Zinc-Ion Battery, *ACS Energy Lett.*, 2021, **6**, 675-683.

10 X. P. Zhang, Y. Y. Liu, P. F. Shen, L. Q. Ren, D. L. Han, M. Feng and H. G. Wang, Engineering an Artificial Coating Layer of Metal Porphyrin-Based Porous Organic Polymers Toward High Stable Aqueous Zinc-Ion Batteries, *Adv. Funct. Mater.*, 2024, **34**, 2400032.

11 Y. P. Wang, Y. D. Yang, S. Q. Duan, L. Wang, J. S. Guo and A. Q. Pan, Anti-corrosive and highly reversible zinc metal anode enabled by the phenolic resin coating, *Rare Metals*, 2024, **43**, 2115-2124.

12 M. H. Zhu, Q. Ran, H. H. Huang, Y. F. Xie, M. X. Zhong, G. Y. Lu, F. Q. Bai, X. Y. Lang, X. T. Jia and D. M. Chao, Interface Reversible Electric Field Regulated by Amphoteric Charged Protein-Based Coating Toward High-Rate and Robust Zn Anode, *Nanomicro Lett*, 2022, **14**, 219.

13 M. Abouali, S. Adhami, S. A. Haris and R. Yuksel, On the Dendrite-Suppressing Effect of Laser-Processed Polylactic Acid-Derived Carbon Coated Zinc Anode in Aqueous Zinc Ion Batteries, *Angew. Chem. Int. Ed.*, 2024, **63**, 202405048.

14 Q. Wen, H. Fu, Y. D. Huang, R. D. Cui, H. Z. Chen, R. H. Ji, L. B. Tang, C. Yan, J. Mao, K. H. Dai, Q. Wu, X. H. Zhang and J. C. Zheng, Constructing defect-free zincophilic organic layer via ultrasonic coating for anticorrosive and dendrite-free zinc anode, *Nano Energy*, 2023, **117**, 108810.

15 Q. Q. Ren, X. Y. Tang, K. He, C. M. Zhang, W. Wang, Y. Q. Guo, Z. X. Zhu, X. F. Xiao, S. Wang, J. Lu and Y. F. Yuan, Long-cycling Zinc Metal Anodes Enabled by an In Situ Constructed ZnO Coating Layer, *Adv. Funct. Mater.,* 2023, **34**, 2312220.

16 F. Tao, K. J. Feng, Y. Liu, J. J. Ren, Y. Xiong, C. B. Li and F. Z. Ren, Suppressing interfacial side reactions of zinc metal anode via isolation effect toward high-performance aqueous zinc-ion batteries, *Nano Res.*, 2022, **16**, 6789-6797.

17 X. Liu, Q. X. Ma, J. H. Wang, Q. Han and C. G. Liu, A Biomimetic Polymer-Based Composite Coating Inhibits Zinc Dendrite Growth for High-Performance Zinc-Ion Batteries, *ACS Appl. Mater. Interfaces*, 2022, **14**, 10384-10393.

18 Z. K. Guo, L. S. Fan, C. Y. Zhao, A. S. Chen, N. N. Liu, Y. Zhang and N. Q. Zhang, A Dynamic and Self-Adapting Interface Coating for Stable Zn-Metal Anodes, *Adv. Mater.*, 2021, **34**, 2105133.

19 H. Zhang, S. Li, L. Q. Xu, R. Y. Momen, W. T. Deng, J. G. Hu, G. Q. Zou, H. S. Hou and X. B. Ji, High-Yield Carbon Dots Interlayer for Ultra-Stable Zinc Batteries, *Adv. Energy Mater.*, 2022, **12**, 2200665.

20 Y. R. Zhou, J. J. Xia, J. T. Di, Z. J. Sun, L. M. Zhao, L. G. Li, Y. L. Wu, L. Z. Dong, X. N. Wang and Q. W. Li, Ultrahigh-Rate Zn Stripping and Plating by Capacitive Charge Carriers Enrichment Boosting Zn-Based Energy Storage, *Adv. Energy Mater.*, 2023, **13**, 2203165.

21 Q. Zong, B. Lv, C. F. Liu, Y. F. Yu, Q. L. Kang, D. Y. Li, Z. J. Zhu, D. W. Tao, J. J. Zhang, J. Y. Wang, Q. L. Zhang and G. Z. Cao, Dendrite-Free and Highly Stable Zn Metal Anode with $BaTiO_3$/P(VDF-TrFE) Coating, *ACS Energy Lett.*, 2023, **8**, 2886-2896.

22 H. Gan, J. Wu, R. Li, B. W. Huang and H. B. Liu, Ultra-stable and deeply rechargeable zinc metal anode enabled by a multifunctional protective layer, *Energy Stor. Mater.*, 2022, **47**, 602-610.

23 Y. P. Wang, X. G. Lin, L. Wang, Y. D. Yang, Y. F. Zhang and A. Q. Pan, Tailoring the Crystal-Chemical States of Water Molecules in Sepiolite for Superior Coating Layers of Zn Metal Anodes, *Adv. Funct. Mater.*, 2023, **33**, 2211088.

24 S. Xia, Q. Y. Luo, J. N. Liu, X. F. Yang, J. Lei, J. J. Shao and X. N. Tang, In Situ Spontaneous Construction of Zinc Phosphate Coating Layer Toward Highly Reversible Zinc Metal Anodes, *Small*, 2024, **20**, 2310497.

25 W. Liu, Q. W. Zhao, H. M. Yu, H. M. Wang, S. Z. Huang, L. J. Zhou, W. F. Wei, Q. C. Zhang, X. B. Ji, Y. J. Chen and L. B. Chen, Metallic Particles-Induced Surface

Reconstruction Enabling Highly Durable Zinc Metal Anode, *Adv. Funct. Mater.*, 2023, **33**, 2302661.

26 D. Y. Xiong, L. Yang, Z. W. Cao, F. R. Li, W. T. Deng, J. G. Hu, H. S. Hou, G. Q. Zou and X. B. Ji, In Situ Construction of High-Density Solid Electrolyte Interphase from MOFs for Advanced Zn Metal Anodes, *Adv. Funct. Mater.*, 2023, **33**, 2301530.

27 L. S. Han, Y. M. Guo, F. H. Ning, X. Y. Liu, J. Yi, Q. Luo, B. H. Qu, J. L. Yue, Y. F. Lu and Q. Li, Lotus Effect Inspired Hydrophobic Strategy for Stable Zn Metal Anodes, *Adv. Mater.*, 2024, **36**, 2308086.

28 H. F. Bian, C. H. Wang, Y. K. Wang, Y. L. Ren, Y. Ge, H. Wu, B. Wang, D. Y. Chen, B. B. Yang, D. Bin, Y. S. Li, J. Gu, Y. J. Ma, S. C. Tang, X. K. Meng and H. B. Lu, Phase Inversion-Induced Porous Polymer Coating for High Rate and Stable Zinc Anode, *Adv. Funct. Mater.*, 2024, **34**, 2401760.